Available online at www.sciencedirect.com

ScienceDirect

Journal of the European Ceramic Society 35 (2015) 2599–2606

www.elsevier.com/locate/jeurceramsoc

Novel highly scalable carbon nanotube-strengthened ceramics by high shear compaction and spark plasma sintering

Konstantinos G. Dassios [a,*], Guillaume Bonnefont [b], Gilbert Fantozzi [b], Theodore E. Matikas [a]

[a] *University of Ioannina, Dept. of Materials Science and Engineering, Ioannina GR-45110, Greece*
[b] *Laboratoire MATEIS, INSA Lyon, 7 Avenue Jean Capelle, 69621 Villeurbanne Cedex, France*

Received 16 December 2014; received in revised form 27 February 2015; accepted 2 March 2015
Available online 26 March 2015

Abstract

We report a new strategy, based on high shear compaction and spark plasma sintering, for the massive and low cost production of 100% dense ceramics containing carbon nanotubes. Custom forming and stacking of flexible green sheets of record-breaking dimensions can yield an unlimited range of three-dimensional structures. The strategy was successfully validated in the production of multi-walled carbon nanotube/Pyrex glass materials of tube loadings in the range of 0–1.5 wt.% while no major factors limit applicability to other types of materials. Improvements in the four elastic constants of the material, Young's modulus, shear modulus, Poisson's ratio and bulk modulus, assessed by means of a non-destructive technique based on ultrasonics, were found maximum at a tube loading of 0.5 wt.% Microstructural investigations indicating the existence of highly dissipating nanoscale-specific toughening mechanisms acting complementary to nanotube bridging and pull-out indicate a high application potential in a wide range of reinforcing and multifunctional applications.

Keywords: Ceramic matrix composites; Nanocomposites; Carbon nanotubes; Glass matrix composites; Elastic properties

1. Introduction

In recent years, increasing amounts of scientific effort concentrate towards exploitation of carbon nanotubes' (CNT) [1] remarkable combination of mechanical [2,3], transport [4–6], optical and electronic properties [7–9] for the development of a new era of ceramics and glasses reinforced at a scale three orders of magnitude closer to molecular dimensions than conventional reinforcements. Property improvement and toughening of the stiff and brittle ceramic monoliths by CNTs depends critically upon four major factors: (i) high tube quality with low impurity content, few structural defects, high crystallinity and high aspect ratios, (ii) establishment of a homogeneous dispersion of nanotubes within the ceramic phase and hampering of CNTs' natural tendency to agglomerate/entangle with extremely undesirable side-effects on material performance, (iii) achievement of appropriate interfacial bonding between the inorganic matrix and the nano-reinforcements to promote toughening through development of energy dissipation mechanisms and (iv) achievement of high densification levels during the final sintering stage [10–12]. All these factors are affected by the manufacturing and processing routes which involve dispersion of the tubes throughout the inorganic continuous phase and sintering of the green material to the high temperatures required for ceramic densification.

Currently suggested tube dispersion technologies in glasses and ceramics include conventional powder processing [13], in situ growth [14], colloidal processing [15] and sol–gel processing [16]. Sintering is achieved either through hot pressing (HP) [17], hot-isostatic pressing (HIP), pressure-less sintering (PS) [18] or spark plasma sintering (SPS) [19]. Due to limitations specific to most aforementioned techniques, achievement of fully dense nanotube-reinforced ceramics, where ultimate material density is – ideally – identical to that of the pure ceramic, is still an open challenge today. For example, the most impressive concept of in situ growth of CNTs in ceramics provides materials with remarkable inherent CNT homogeneity that may, nonetheless, suffer from incomplete sinterability

* Corresponding author. Tel.: +30 26510 09010; fax: +30 26510 09066.
E-mail address: kdassios@cc.uoi.gr (K.G. Dassios).

http://dx.doi.org/10.1016/j.jeurceramsoc.2015.03.003
0955-2219/

due to CNTs pinned at grain boundaries blocking densification [16]. On the other hand, PS suffers from the requirement of extremely hostile – for the nanotubes – temperatures, above 1300 °C, to yield fully dense ceramics [17]. In H(I)P and PS, heat provided externally to the sample is frequently associated with non-uniform sintering pattern throughout material volume. Among sintering methods, SPS stands out for being associated with higher final densities, lower sintering temperatures and shorter processing durations, hence leading to ceramics of superior properties [13,20–22]. In one notable case, a fully dense nanotube-alumina ceramic with unprecedented toughening characteristics was recently processed via SPS by Estili et al. [23]. Lowering of production costs and upscaling of production rates of CNT–ceramics that will unfold their application potential are also issues that remain to be resolved.

Here, we propose a completely new, highly scalable, low cost methodology for large scale production of 100% dense carbon nanotube-reinforced ceramics starting from flexible green (unfired) sheets of ceramic powder and homogeneously embedded nanotubes bound by high shear compaction (HSC). HSC is a state of the art, continuous production tape forming process, wherein powders are closely packed by water-based binders subject to high shear forces while the material is maintained at a very high viscosity. HSC is superior to other tape forming processes including tape casting, roll compaction, slip casting and powder pressing in that (i) it allows density prediction by control of degree of compaction, (ii) particles and fillers embedded in the continuous phase cannot settle hence non-uniform particle size distribution typical with casting technologies is prevented, (iii) continuous phase powder grains sheared against one another close-pack to green densities higher than any other tape forming process, a feature which tremendously aids sinterability, (iv) resultant sheets are completely isotropic with greatly reduced fired shrinkage variation and, (v) they are flexible enough to enable post-forming into complex shapes.

Green CNT–glass sheets of record-breaking surface areas of 0.5 m^2 were manufactured during this study while the process is scalable to an impressive sheet surface area of 350 m^2 of widths up to 8 m at a production rate of 1.5 m/min. The green product is flexible enough to allow forming into virtually any geometry and stacking for the production of an unlimited range of three-dimensional structures. Green CNT–ceramic disks of varying nanotube loadings underwent a single-step SPS cycle for binder burnout and sintering during which unconventional densification levels, to 100% of the pure ceramic, were achieved. A borosilicate Pyrex glass was utilized as continuous phase and long multi-walled CNTs as reinforcement while no apparent factors limit applicability of the technique to other phases or hybrid materials. The material exhibited significant stiffness improvement under both shear and axial elastic loads while indications of nano-scale and micro-scale toughening mechanisms indicate high application potential of the material and stimulate further research.

2. Experimental procedures

Pyrex borosilicate glass, Corning code 7740, a low expansion glass resistant to chemical attack and conforming to ASTM E-438, was provided in powder form by Corning Refractories (Corning, NY, USA). The nominal density, Young's modulus, shear modulus and Poisson's ratio of the glass are 2.23 g/cm^3, 64 GPa, 26.7 GPa and 0.2, respectively. Multi-wall carbon nanotubes (MWCNT) of nominal purity higher than 97% and amorphous carbon content of less than 3%, synthesized via catalytic chemical vapor deposition were acquired by Shenzhen Nanotech Port Co. Ltd. (Shenzhen, China). Nominal tube diameter ranged from 20 to 40 nm while their length ranged from 5 to 15 μm.

Our strategy for fabrication of fully dense MWCNT/Pyrex borosilicate glass is summarized in Fig. 1. Therein, surfactant-assisted aqueous suspensions of the tubes were initially prepared by addition of sodium dodecyl sulphate (SDS, Sigma–Aldrich code 436143, Sigma–Aldrich Chemie Gmbh, Munich, Germany) and of MWCNTs, at an 1/1 weight ratio, in 1500 cm^3 (1.5 l) triple-distilled water in standard Pyrex glass beakers and subsequent ultrasonic processing at a frequency of 24 kHz, for 20 min. A Ø22 mm cylindrical sonotrode operating on a Hielscher UP400S device (Hielscher Ultrasonics GmbH, Teltow, Germany) delivered a power throughput of 4500 J/min to the tubes. The specific combination of ultrasonic energy and processing duration was established as optimum for achievement of homogeneous dispersions of the tubes in the target volume without significant degradation of their initial length. The latter task involved a tedious parametric analysis of CNT agglomerate size variation with ultrasonication time and energy, by laser diffraction [30].

Using the nominal borosilicate glass density value of 2.23 g/cm^3, appropriate amounts of aqueous MWCNT suspensions were calculated al and added to the HSC binder to yield sheets of variable CNT loadings within 0–1.5 wt.%, step of 0.25 wt.%. The resultant MWCNT/Pyrex green sheets of unprecedentedly highly surface areas of 0.5 m^2 per formulation, thickness of 3 mm, were cut into 125 mm × 125 mm green plates.

Sets of four 20 mm diameter disks were cut from the plates at each MWCNT formulation; the disks were stacked and sintered in a SPS HPD 25/1 machine (Fine Ceramics Technologies GmbH, Germany) equipped with a graphite die of an internal diameter of 20 mm. All experiments were performed under vacuum of 8×10^{-2} mbar, a standard feature of the technique which proved indispensable for the needs of the current study, namely in preventing carbon nanotube oxidation/loss during residence of the material at the high temperatures required for sintering and densification of the borosilicate glass. A punch pressure was applied to all samples before heating and was retained through the entire thermal cycle duration; pressure was gradually removed during cooling. A pulse sequence consisting of 10 ms of pulse current followed by 5 ms of current without pulse, was chosen. To identify the optimal sintering temperature for achievement of fully dense samples, the real-time densification rate of the ceramic, quantified by means of displacement speed of the mobile upper punch of the apparatus, was investigated. Bulk densities of samples were measured through Archimedes' method following standard protocol ASTM C373-88. The thermal cycle used for all

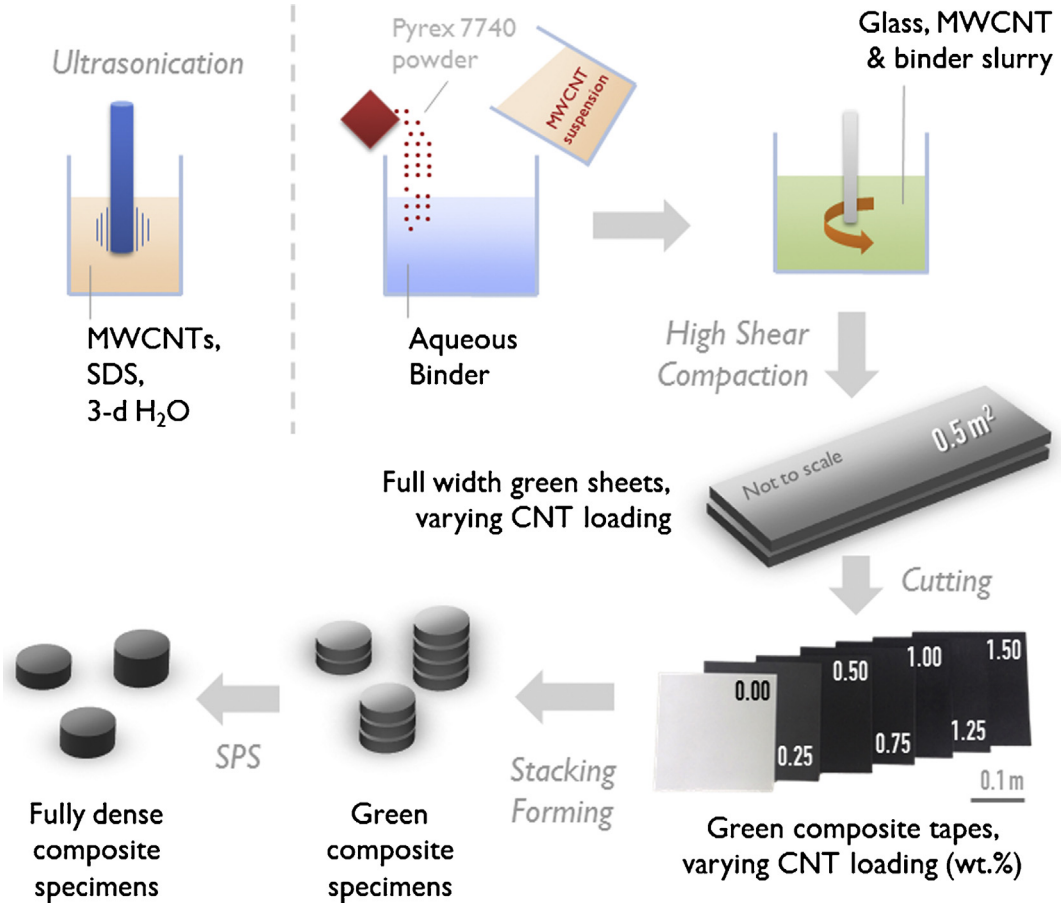

Fig. 1. Graphical overview of proposed route for fabrication of MWCNT ceramics.

specimens consisted of four stages: initial heating to 200 °C with a rate of 100 °C/min; followed by heating to 300 °C at a rate of 10 °C/min; then heating to 500 °C at a rate of 5 °C/min and the final heating stage consisted of heating to the target sintering temperature (600, 650, or 700 °C) at a rate of 15 °C/min. Samples were not allowed soaking time at the sintering temperature; a natural cooling step, duration of ca. 10 min, completed the thermal cycle. The total duration of the thermal cycles was ca. 90 min. Obtained CNT/Pyrex samples had a thickness of 4.5 ± 0.1 mm after SPS; the associated degree of axial compaction from the initial green state was calculated as 68%.

The four elastic constants of the sintered compacts, namely, Young's modulus, shear modulus, bulk modulus and Poisson's ratio were measured non-destructively at zero-load by the ultrasonic methodology described in [24]. In brief, the velocities of propagation of ultrasonic waves – which are elastic stresses of small amplitude – are directly related to the elastic moduli of the material at zero-load (dynamic moduli). Knowledge of shear and longitudinal velocities, makes feasible the computation of all four elastic constants through equations 7–10 in [24]. In the current study, ultrasonic wave velocities were measured using piezoelectric transducers with *x*-cut or *y*-cut crystals, for longitudinal and shear wave generation, respectively, operating in pulse-echo mode. Ultrasonic frequencies of 15 and 5 MHz were used for longitudinal and shear waves, respectively, with provision for ultrasound wavelength to remain much smaller than specimen thickness. The microstructure of polished surfaces of CNT–ceramic specimens was examined in a Zeiss SUPRA 35VP scanning electron microscope equipped with a 30 kV electron beam.

3. Results and discussion

Given the detrimental effect of incomplete densification on ceramic performance, tuning of sintering parameters for the achievement of fully dense samples was a key concern of the present study. In terms of punch pressure, typical values of 16 and 32 MPa were tested and the latter was favored as it was found associated with higher ceramic densification levels. Higher pressure values were considered potentially harmful to the brittle material's integrity and were not tested. Optimal sintering temperature was established by examination of the real-time densification curves of the ceramics as shown in Fig. 2. It was observed that densification began at ca. 500 °C, was maximum at ca. 570 °C (nominal annealing temperature for Pyrex 7740 is 560 °C) and complete at ca. 630 °C. CNT–ceramics sintered at 650 °C were found to be fully dense. A much narrower peak, appearing at ca. 330 °C in the densification curves was associated with binder burnout, i.e. the very fast decomposition of the material holding the glass grains and tubes tightly bound.

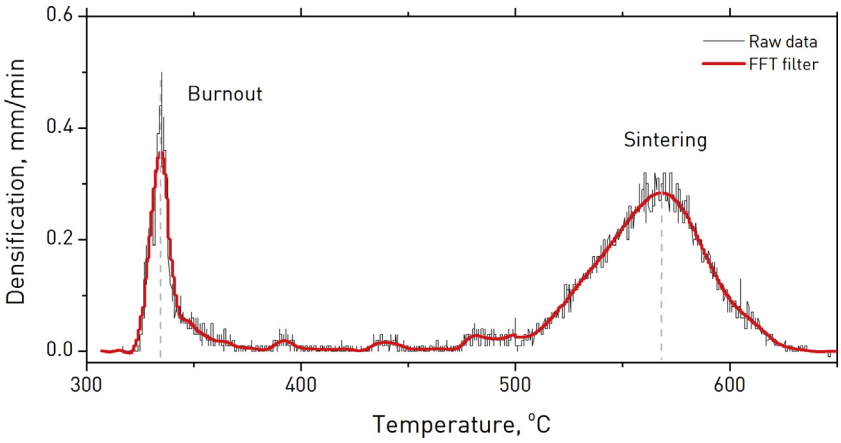

Fig. 2. Real-time densification rate of MWCNT/borosilicate glass as function of temperature during SPS cycle.

To demonstrate the actual effect of sintering temperature on densification, hence also material performance, three final sintering temperatures of 600, 650 and 700 °C were investigated; the resulting levels of densification, are plotted as a function of tube loading for all seven MWCNT formulations (0–1.5 wt.%, step of 0.25 wt.%) in Fig. 3. It is observed that sintering at 600 °C yielded only partially densified samples with property values appearing systematically lower than both the fully dense case and their 650 and 700 °C counterparts. Samples sintered at 650 °C were found to be fully dense within the entire nanotube loading range up to 1.25%; density dropped by 0.9% in the ceramic with the maximum MWCNT content, 1.5 wt.%. A sintering temperature of 700 °C appeared to offer similar densification efficiency, however the surprising low densities returned for the pure-borosilicate sample and for the 1.5 wt.% loaded samples did not favor selection of the particular temperature. Contrary to conventional sintering techniques, which involve successive thermal cycles for binder burn-out, sintering and densification, the single-step SPS cycle proposed in the current work is highly efficient, fully customizable and time saving.

The variation of dynamic moduli of MWCNT/Pyrex specimens sintered at 600, 650 and 700 °C is plotted in Fig. 4a and b as a function of sintering temperature and nanotube concentration in the compacts. For samples sintered at 600 °C (data represented in red solid square symbols) both property values appeared lower than their nominal pure Pyrex 7740 glass counterparts; this behavior is believed to be directly associated with the low densification level of the particular samples due to incomplete sintering at 600 °C. Nonetheless, a prominent increase in both moduli appears to occur at 0.5 wt.% MWCNT loading, followed by a steep property degradation thereafter. Similar enhancements, in both moduli, for 0.5 wt.% tube loading were noted for the fully dense ceramics sintered at 650 °C, as Fig. 4a and b suggests (red solid cycle symbols). For these samples, the

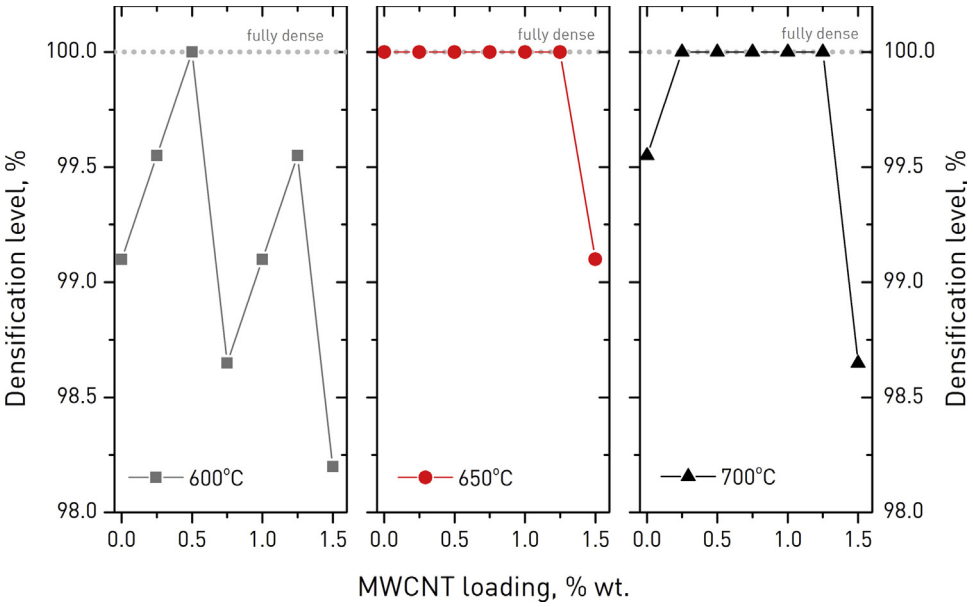

Fig. 3. Densification levels of MWCNT/borosilicate glass materials with varying nanotube concentrations as a function of sintering temperature (600, 650 and 700 °C). The *y*-axis values are obtained by normalization of CNT/ceramic densities measured via the Archimedes method, to 2.22 g/cm^3, the property value achieved for fully dense pure borosilicate glass samples (0% MWCNT loading).

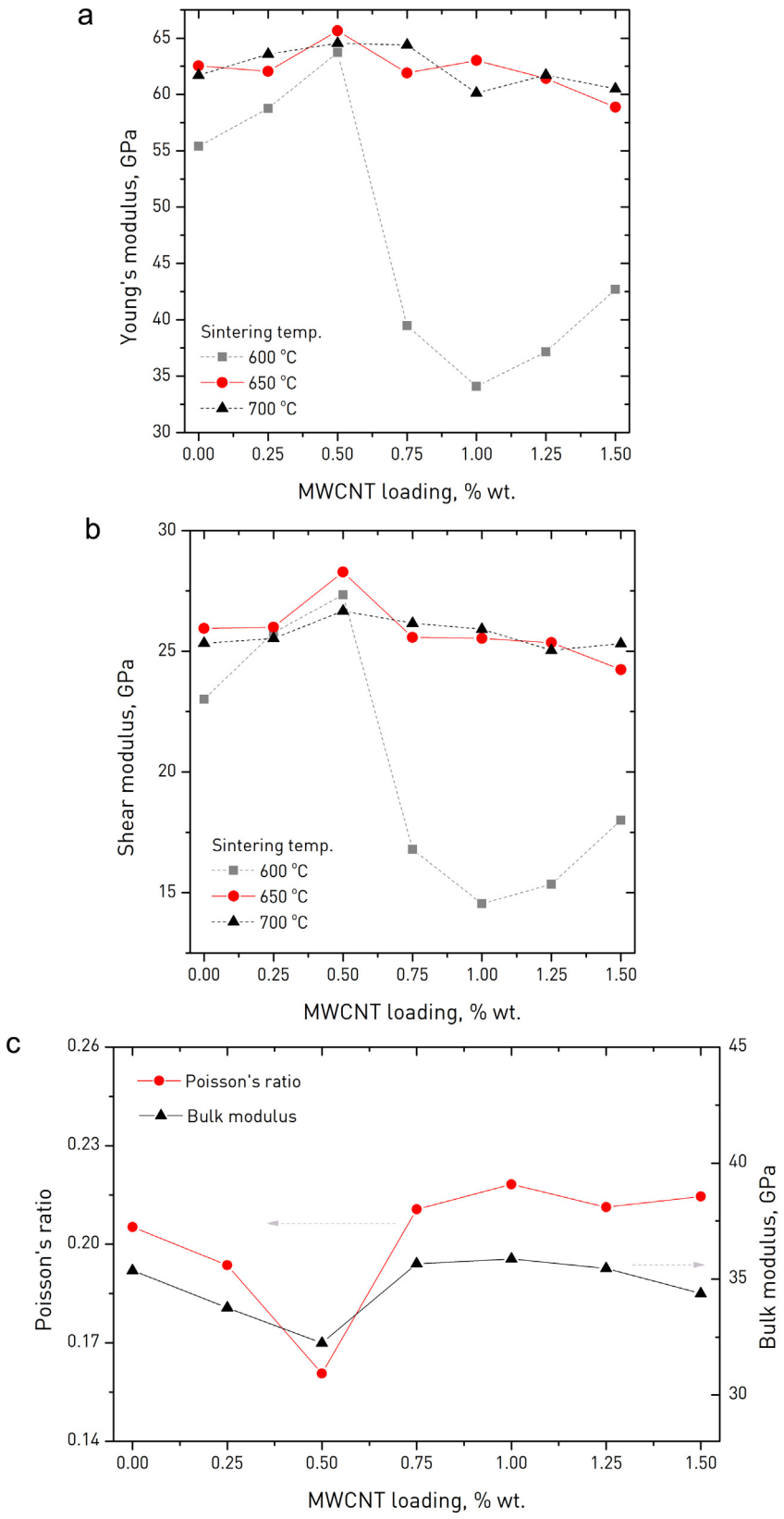

Fig. 4. Dynamic mechanical properties of MWCNT/borosilicate glass versus tube loading: (a) Young's modulus, (b) shear modulus for samples sintered at 600, 650 and 700 °C and (c) Poisson's ratio (red solid cycle symbols) and bulk modulus (black solid triangle symbols) of fully dense samples sintered at 650 °C. (For interpretation of the references to color in this figure legend, the reader is referred to the web version of this article.)

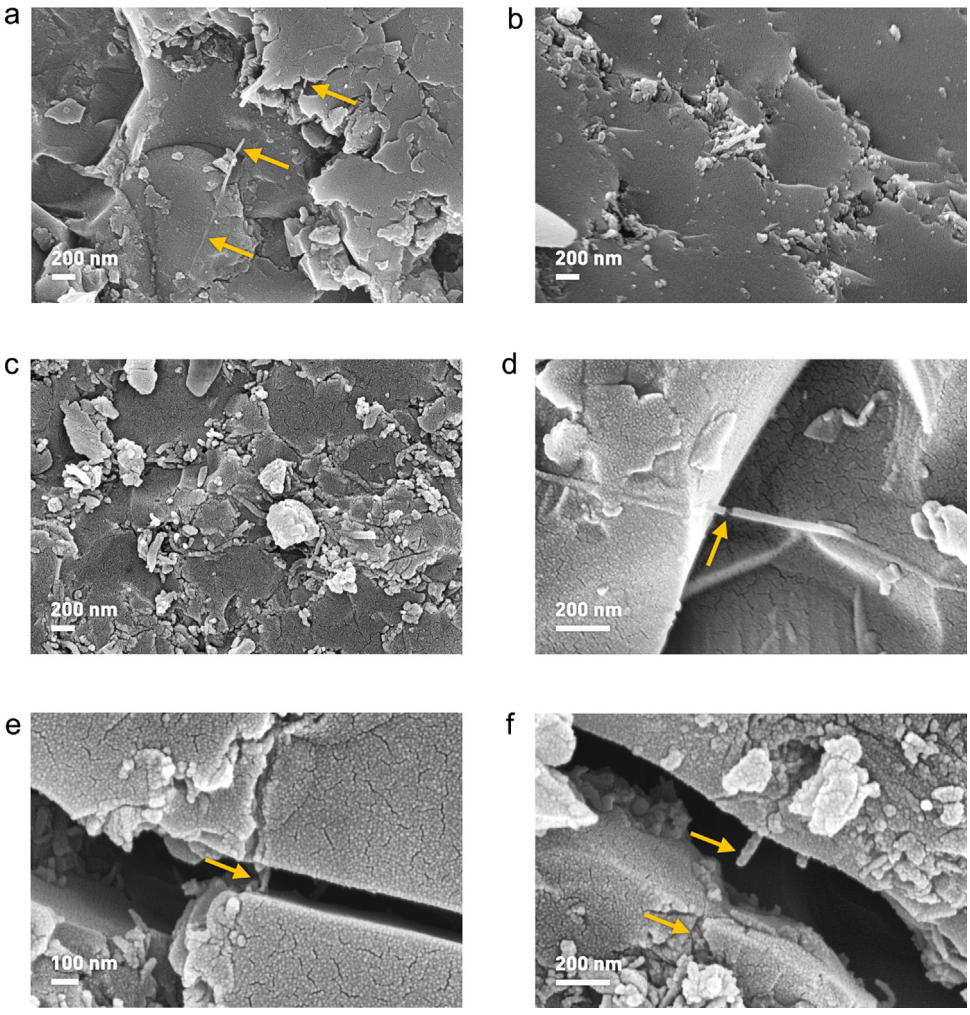

Fig. 5. SEM micrographs of surfaces of MWCNT/borosilicate glass sintered at 650 °C. Unless otherwise noted, MWCNT loadings are indicated in parentheses after each caption: (a) exposed tube surfaces and tips (0.5 wt.%), (b) agglomeration pockets in a 1.00 wt.% sample and (c) worsely agglomerated state in a 1.50 wt.% loaded sample, (d) multiwall-type nanotube failure (0.5 wt.%), (e) crack bridging by intact nanotubes (1.5 wt.%) and (f) nanotube pull-out (1.5 wt.%). The fine craquelure pattern visible in high magnification micrographs d–f, is artifact of the SEM-prone Au-sputter coating and is not part of material morphology.

values of Young's and shear modulus at 0% loading, 62.5 and 25.9 GPa respectively, compared favorably to the nominal values reported by the glass manufacturer, 64 and 26.7 GPa respectively. Corresponding peak property values at 0.5 wt.% loading were 65.7 and 28.5 GPa respectively, increased by 5% and 10% respectively, from their pure-glass counterparts. Both property values appeared to drop to the previous levels as tube concentrations increased above 0.5 wt.%. Moduli enhancements were less prominent in MWCNT/Pyrex specimens sintered at 700 °C, where a 5.4% increase was noted in shear modulus at 0.5 wt.% loading and a 4.3% increase in Young's modulus was found shifted to 0.75 wt.% loading. The observed tendency, of property enhancements being limited at low nanotube loading fractions and of further increases in concentration leading to opposite effects, is not an unknown phenomenon for CNT–reinforced ceramics and is attributed to CNT dispersion deficiency due to enabling of tube agglomerates formation at high loadings [11,12]. In this context, the very steep drop in moduli observed for samples sintered at 600 °C can be rationalized upon the combined effect of incomplete sintering and agglomeration.

The variation of Poisson's ratio and bulk modulus is plotted in Fig. 4c as a function of nanotube loading, for the CNT/Pyrex fully densified at 650 °C. Both properties are observed to reach *minima* at the tube concentration previously found associated with the *maximum* improvement in moduli, i.e. 0.5 wt.%. This seemingly unconventional behavior, signifies that both the ceramic's resistance to uniform pressure and the ratio of transverse to axial deformation are least when material resistances to axial and shearing stresses are greatest. In fact, such a condition is not incompatible with theory of elasticity expectations. Therein, Young's modulus, E, is related to bulk modulus, K, and Poisson's ratio, ν, through:

$$E = 3K(1 - 2\nu) \tag{1}$$

In Eq. (1), for minimization of ν, the negative term 2ν can maximize enough to dominate over K minimization, so that the product on the right-hand side of Eq. (1), i.e. the material's

resistances to axial stress can indeed maximize. Likewise, shear modulus, G, is related to K and ν through

$$G = \frac{3K(1-2\nu)}{2(1+\nu)} \quad (2)$$

Here, minimization of ν leads to the simultaneously maximization of both $(1-2\nu)$ and reciprocal $2(1+\nu)$, hence the fraction on the right-hand side of Eq. (2), i.e. the material's resistances to shear stress, maximizes more rapidly than in the previous case. This may also explain the higher improvement (10%) noted for the shear modulus at 0.5 wt.% loading, compared to the elastic modulus (5%), for CTN/ceramics sintered at 650 °C.

Typical morphologies of fully dense CNT/Pyrex samples sintered at 650 °C are presented in Fig. 5. Two important overall observations were that tube integrity appeared unaffected by the high shear/high temperature sintering process and that good wetting between the tubes and the ceramic was achieved. The latter observation is particularly significant in view of the toughening potential of the tubes which requires a poreless interface with the ceramic environment to allow development of energy dissipation mechanisms [25]. Tube population density clearly increased with loading and, in many cases, large parts of the tubes lengths were exposed on the surfaces under observation, as for example in the 0.5 wt.% MWCNT-loaded sample depicted in Fig. 5a. No indications of tube dispersion inhomogeneity or agglomeration were observed for loadings below 0.75 wt.%. Above this concentration, pockets of entangled tubes were evident; their magnitude increased with tube concentration, as seen in Fig. 5b and c taken from samples with CNT loadings of 1.00 and 1.50 wt.%, respectively. Indications of existence of toughening mechanisms around small microcracks and ceramic crystal boundaries were observed at most MWCNT loadings. Fig. 5d demonstrates the failure of a single bridging nanotube in a sample with 0.50 wt.% tube content; a large part of tube length is visible on the surface. While such bridging phenomena already constitute a fundamental toughening/energy-dissipating mechanism for composites [26,27], a more careful observation at the failure location reveals a very interesting effect wherein a number of central graphene walls remain intact to partially connect the otherwise separating tips of a failed tube. This multiwall type of failure was very recently discovered to endow high energy-dissipating potential and unprecedented toughening to MWCNT/alumina ceramics [23]. In fact, in a new era of CNT-reinforced matter where the effects of a thousandfold diameter reduction are yet unclear, the specific mechanism is, along with friction due to pull-out of wavy or buckled tubes [28,29], the only nanoscale-specific toughening mechanisms suggested to date. Indications of existence of such multiwall-type of failure in our material, coupled with findings of nanotube bridging and pull-out as seen in Fig. 5e and f, imply a high energy-dissipation potential which could be exploited for the enhancement of fracture toughness, crack growth resistance and strain tolerance of the ceramic under investigation and, quite possibly, of many other ceramics and glasses. At the same time, manufacturing of CNT–ceramics at full scales, custom geometries, low costs and high production rates can unfold advances toward complex design of high-performance components for electronic, structural, optical, biomedical and high temperature applications. To the best of our knowledge CNT–ceramic manufacturing rates and dimensions similar to the ones proposed in the present methodology have not been previously reported in the literature and are a result of the efficient production route suggested herein. At the same time, final densification levels above current standards are reached due to close packing and unprecedentedly high green densities achieved by the proposed HSC technique.

4. Conclusions

We report a new, highly scalable and sustainable strategy which opens the doors for low cost and massive production of full scale nanotube-strengthened ceramics and glasses. Custom forming and stacking of flexible HSC-bound green CNT–ceramic sheets of record-breaking dimensions can yield an unlimited range of three-dimensional structures while no apparent factors limit application of the technique to reinforcements, continuous media or hybrid materials different than the MWCNTs and Pyrex 7740 borosilicate glass utilized herein. The technique was systematically found associated with 100% dense final materials which dramatically improves current CNT–ceramic densification standards. MWCNT loadings of 0.5 wt.% provided optimal stiffness improvement of the borosilicate glass under both shear and axial elastic loads while indications of nanoscale-specific energy dissipation mechanisms stimulate further research on the toughening and functional aspects of the material for a wide range of reinforcing and multifunctional applications.

Acknowledgements

William Belko, President of Ragan Technologies Inc., MA, USA, is thankfully acknowledged for the production, under HSC, of the green tapes. Ms. Mary Lou Schwartz of Corning Refractories, NY, USA and Dr. Apel Horst of Corning GmbH, Wiesbaden, Germany are gratefully thanked for providing the Pyrex 7740 borosilicate glass in this study. The support of Natural Science Foundation of China (51272210 and 50902112) is acknowledged.

References

[1]. Iijima S. Helical microtubules of graphitic carbon. *Nature* 1991;**354**:56–8.
[2]. Treacy MMJ, Ebbesen TW, Gibson JM. Exceptionally high Young's modulus observed for individual carbon nanotubes. *Nature* 1996;**381**:678–80.
[3]. Yu MF, Lourie O, Dyer MJ, Moloni K, Kelly TF, Ruoff RS. Strength and breaking mechanism of multiwalled carbon nanotubes under tensile load. *Science* 2000;**287**:637–40.
[4]. Balandin AA. Thermal properties of graphene and nanostructured carbon materials. *Nat Mater* 2011;**10**:569–81.
[5]. Berber S, Kwon YK, Tomanek D. Unusually high thermal conductivity of carbon nanotubes. *Phys Rev Lett* 2000;**84**:4613–6.
[6]. Baughman RH, Zakhidov AA, de Heer WA. Carbon nanotubes – the route toward applications. *Science* 2002;**297**:787–92.
[7]. Berber S, Kwon YK, Tomanek D. Electronic and structural properties of carbon nanohorns. *Phys Rev B* 2000;**62**:R2291–4.

[8]. Avouris P, Chen ZH, Perebeinos V. Carbon-based electronics. *Nat Nanotechnol* 2007;**2**:605–15.
[9]. Avouris P, Freitag M, Perebeinos V. Carbon-nanotube photonics and optoelectronics. *Nat Photonics* 2008;**2**:341–50.
[10]. Cho J, Inam F, Reece MJ, Chlup Z, Dlouhy I, Shaffer MSP, et al. Carbon nanotubes: do they toughen brittle matrices? *J Mater Sci* 2011;**46**:4770–9.
[11]. Dassios KG. Carbon nanotube–reinforced ceramic matrix composites: processing and properties. *Ceram Trans* 2014;**248**:133–57.
[12]. Cho J, Boccaccini AR, Shaffer MSP. Ceramic matrix composites containing carbon nanotubes. *J Mater Sci* 2009;**44**:1934–51.
[13]. Inam F, Yan HX, Peijs T, Reece MJ. The sintering and grain growth behaviour of ceramic–carbon nanotube nanocomposites. *Compos Sci Technol* 2010;**70**:947–52.
[14]. Peigney A, Laurent C, Flahaut E, Rousset A. Carbon nanotubes in novel ceramic matrix nanocomposites. *Ceram Int* 2000;**26**:677–83.
[15]. Estili M, Kawasaki A. An approach to mass-producing individually alumina-decorated multi-walled carbon nanotubes with optimized and controlled compositions. *Scripta Mater* 2008;**58**:906–9.
[16]. Thomas BJC, Shaffer MSP, Boccaccini AR. Sol–gel route to carbon nanotube borosilicate glass composites. *Compos A Appl Sci* 2009;**40**:837–45.
[17]. Peigney A, Rul S, Lefevre-Schlick F, Laurent C. Densification during hot-pressing of carbon nanotube–metal–magnesium aluminate spinel nanocomposites. *J Eur Ceram Soc* 2007;**27**:2183–93.
[18]. Du HB, Li YL, Zhou FQ, Su D, Hou F. One-step fabrication of ceramic and carbon nanotube (CNT) composites by in situ growth of CNTs. *J Am Ceram Soc* 2010;**93**:1290–6.
[19]. Dobedoe RS, West GD, Lewis MH. Spark plasma sintering of ceramics: understanding temperature distribution enables more realistic comparison with conventional processing. *Adv Appl Ceram* 2005;**104**:110–6.
[20]. Hvizdos P, Puchy V, Duszova A, Dusza J, Balazsi C. Tribological and electrical properties of ceramic matrix composites with carbon nanotubes. *Ceram Int* 2012;**38**:5669–76.
[21]. Tapaszto O, Kun P, Weber F, Gergely G, Balazsi K, Pfeifer J, et al. Silicon nitride based nanocomposites produced by two different sintering methods. *Ceram Int* 2011;**37**:3457–61.
[22]. Zhang SC, Fahrenholtz WG, Hilmas GE, Yadlowsky EJ. Pressureless sintering of carbon nanotube–Al_2O_3 composites. *J Eur Ceram Soc* 2010;**30**:1373–80.
[23]. Estili M, Sakka Y, Kawasaki A. Unprecedented simultaneous enhancement in strain tolerance, toughness and strength of Al_2O_3 ceramic by multiwall-type failure of a high loading of carbon nanotubes. *Nanotechnology* 2013:24.
[24]. Matikas TE, Karpur P, Shamasundar S. Measurement of the dynamic elastic moduli of porous titanium aluminide compacts. *J Mater Sci* 1997;**32**:1099–103.
[25]. Estili M, Kawasaki A, Sakka Y. Highly concentrated 3D macrostructure of individual carbon nanotubes in a ceramic environment. *Adv Mater* 2012;**24**:4322.
[26]. Dassios KG, Galiotis C. Direct measurement of fiber bridging in notched glass–ceramic-matrix composites. *J Mater Res* 2006;**21**:1150–60.
[27]. Dassios KG, Kostopoulos V, Steen M. A micromechanical bridging law model for CFCCs. *Acta Mater* 2007;**55**:83–92.
[28]. Xia Z, Riester L, Curtin WA, Li H, Sheldon BW, Liang J, et al. Direct observation of toughening mechanisms in carbon nanotube ceramic matrix composites. *Acta Mater* 2004;**52**:931–44.
[29]. Gu ZJ, Yang YC, Li KY, Tao XY, Eres G, Howe JY, et al. Aligned carbon nanotube–reinforced silicon carbide composites produced by chemical vapor infiltration. *Carbon* 2011;**49**:2475–82.
[30]. Dassios KG, Alafogianni P, Antiohos SK, Leptokaridis C, Barkoula NM, Matikas TE. Optimization of Sonication Parameters for Homogeneous Surfactant-Assisted Dispersion of Multiwalled Carbon Nanotubes in Aqueous Solutions. *J Phys Chem* http://dx.doi.org/10.1021/acs.jpcc.5b01349, [In Press].